Supplementary Figures Gao, Daneva, et al.

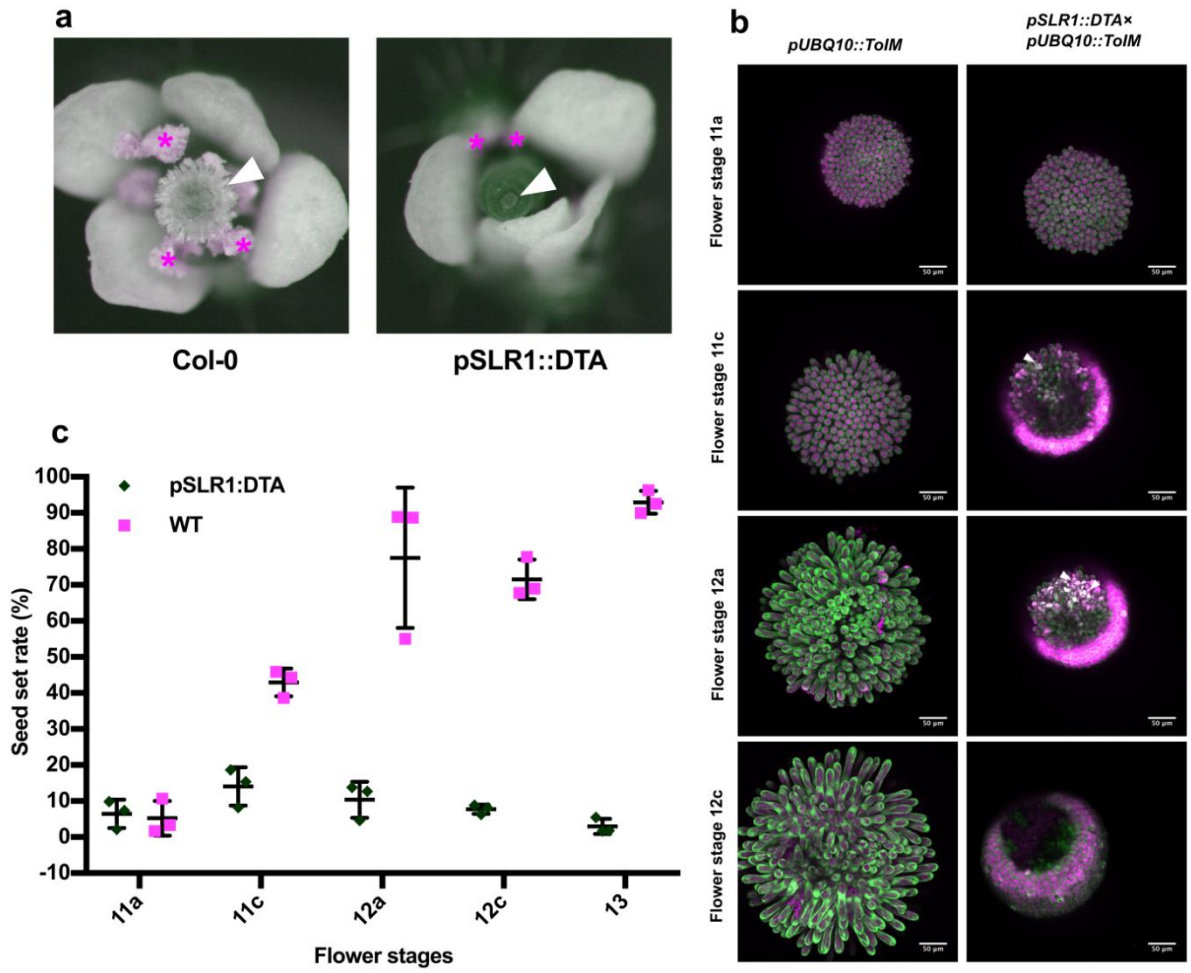

Figure S1: Stigma-specific *DT-A* expression leads to papilla cell death and loss of floral receptivity. a) Macroscopic photography showing a Col-0 wild-type flower at stage 13 (anthesis), and a representative transgenic *pSLR1::DT-A* flower at a comparable stage. Note the degenerated stigma (arrowheads), and the underdeveloped anthers (asterisks). **b)** Maximum projections of wild-type (left) and *DT-A* expressing (right) stigmata expressing a tonoplast integrity marker (*TolM*, expressing cytoplasmic GFP and vacuolar localized RFP[1]). Whereas no difference between wild type and *DT-A*-expressing flowers is visible at flower stage 11a, in subsequent stages a stop of development and a progressive degeneration of papilla cells (merging of magenta and green fluorescence, arrowheads) can be seen. **c)** A pollination assay at the same stages as shown in B demonstrates a progressive loss of floral receptivity correlated with stigma ablation by DT-A. The magenta squares show that the seed set in Col-0 wild-type increased from flower stage 11a until flower stage 13 (mean±SD=5.23±4.80%, 42.93±3.84%, 77.53±19.52%, 71.53±5.46%, 92.93±3.17%). The green squares show the seed set in *pSLR1::DT-A* during flower development from flower stage 11a until flower stage 13 (mean±SD=6.43±3.94%, 14.04±5.31%, 10.37±5.02%, 7.73±1.29%, 2.97±2.11%). Error bars show the standard deviation, n=3, $p<0.05$ from flower stage 11c to stage 13. Scale bars, 50 µm.

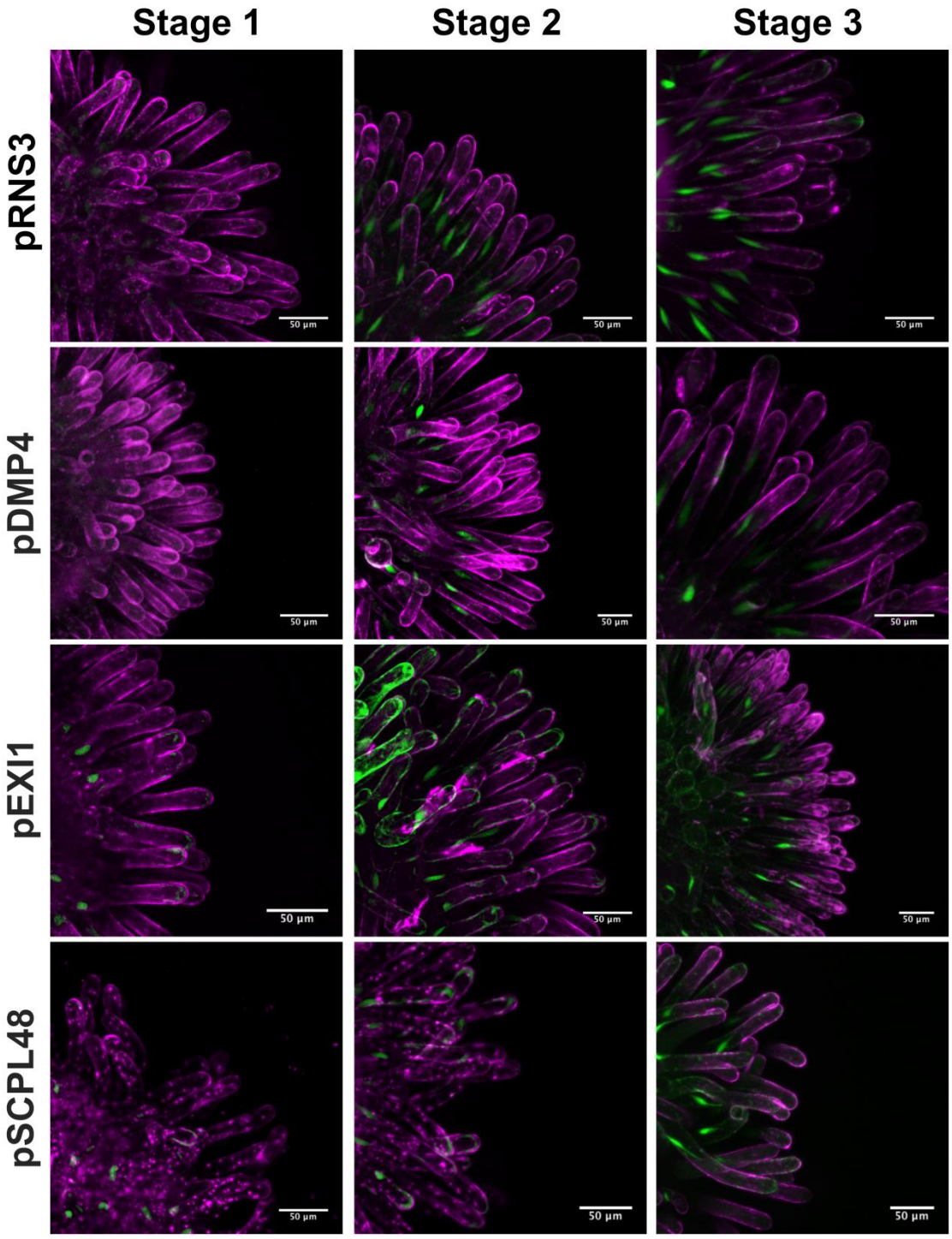

Figure S2. Additional promoter-reporters of dPCD-associated genes are expressed during stigma senescence. Confocal maximum projections of papilla cells at different stages of stigma senescence show an increased expression of a nuclear-localized H2A-GFP signal (green), contrasted with magenta PI staining of the cell walls. Scale bars, 50 µm.

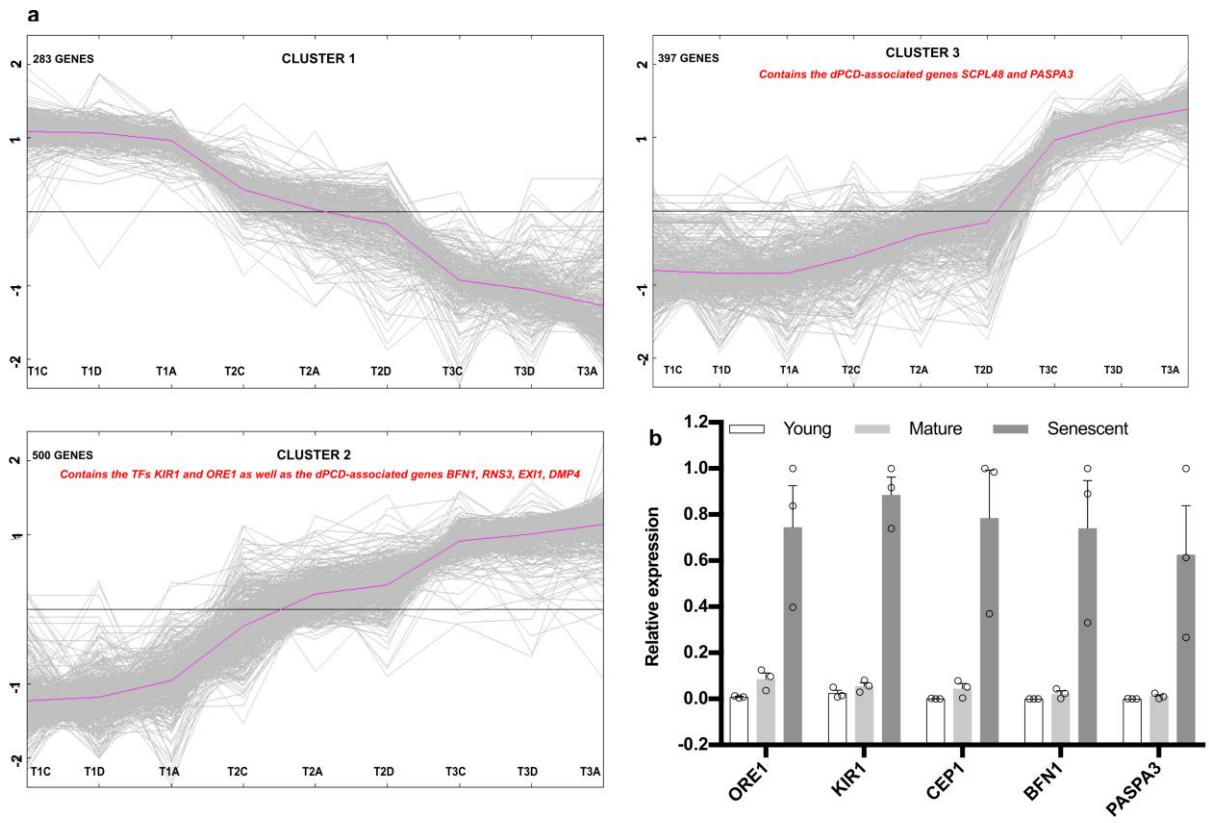

Figure S3. *ORE1* and *KIR1* are co-regulated with dPCD-associated genes. a) A cluster analysis reveals three co-expression clusters within the RNA-Seq data of stigma development. Cluster 1 contains down-regulated genes, while Cluster 2 harbors major dPCD genes, which are co-expressed together with the transcription factors ORE1 and KIR1 (see Table S1). Some late dPCD genes also fall into Cluster 3. Labels on the x-axis show time points (T1-3) and replicates (A-D). Thy y-axis shows Log_2 scale from -2 to 2. **b)** qPCR confirms the common upregulation of *ORE1*, *KIR1* and the dPCD-associated genes *CEP1*, *BFN1*, and *PASPA3* in senescent stigmata. Mean values of three biological replicates are represented (n=200 per replicate); expression values are relative to the reference genes *ACTIN2* and *EEF1A4*.

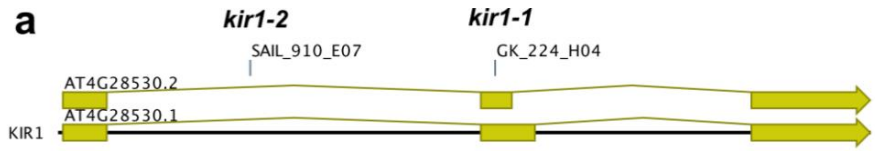

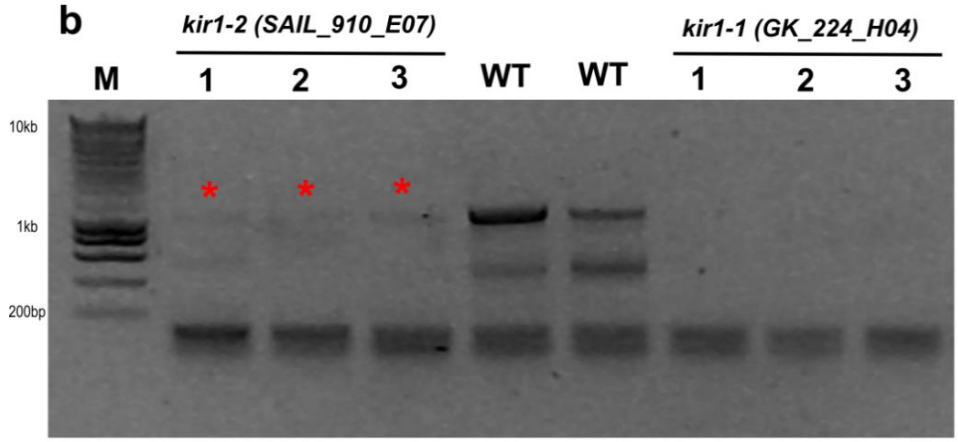

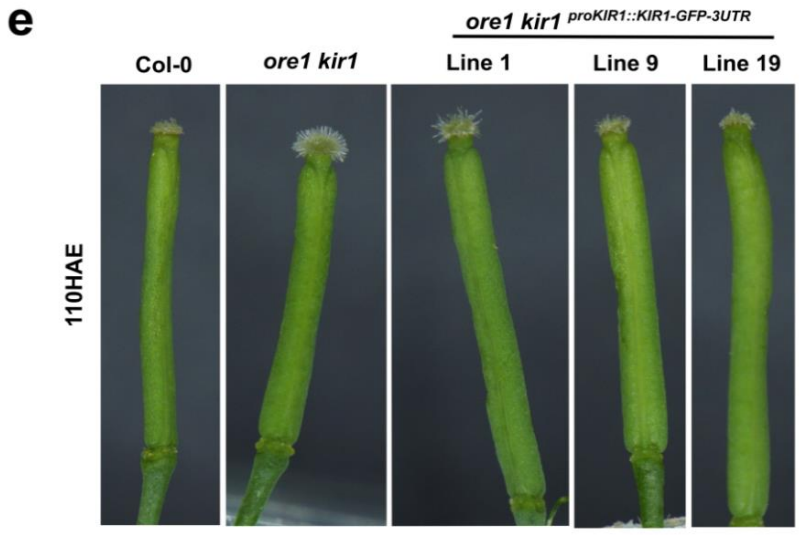

f

GENOTYPE	INTACT	COLLAPSING	FULLY COLLAPSED
ore1 kir1	16	6	0
Col-0	0	4	23
Complemented *LINE1*	3	27	2
Complemented *LINE9*	0	1	49
Complemented *LINE19*	0	6	28

Figure S4. *Kir 1* mutant characterization. a) Putative T-DNA insertion loci of two *kir1* mutant alleles. Note that the SAIL mutant contains a T-DNA insertion in the large first intron of *KIR1*, whereas the GABIKAT (GK) allele matches the second exon. Introns are presented by thin black lines, exons by boxes. **b)** RT-PCR reveals lack of full-length (~ 1500 bp) *KIR1* transcripts in three homozygous GK plants. The full-length *KIR1* transcript present in WT is marked with white asterisks. Note that faint bands are present in all three tested homozygous SAIL plants (red asterisk). M, DNA marker 200bp-10kb; WT, wild type. **c)** Snapshots of flower and stigma development from a representative *kir 1-2* flower taken at 24-, 48-, 72- and and 96HAE. **d)** A comparison of stigma lifespan in the *kir 1-2* mutant and Col-0 control. One biological replicate is shown, n=5 per genotype; mean±SD=58.8±10.5h for Col-0 and mean±SD=68.14±8.06h for *kir 1-2*. **e)** A genetic rescue of the long-living stigma phenotype of the double *ore1 kir1* mutant with the translational reporter *proKIR1::KIR1-GFP-3UTR*. While at 110HAE the stigma of the double mutant *ore 1 kir1* is still viable, the wild type stigma appears completely collapsed. The complemented Lines 1, -9 and - 19 show different degrees of complementation, with Line 1 being only partially rescued. **f)** A table view of the complementation experiment shown in **e)**. Three categories describe macroscopic stigma appearance (intact, collapsing and fully collapsed). The experiment was repeated 3 times with a minimum of 6 flowers per repeat and per genotype.

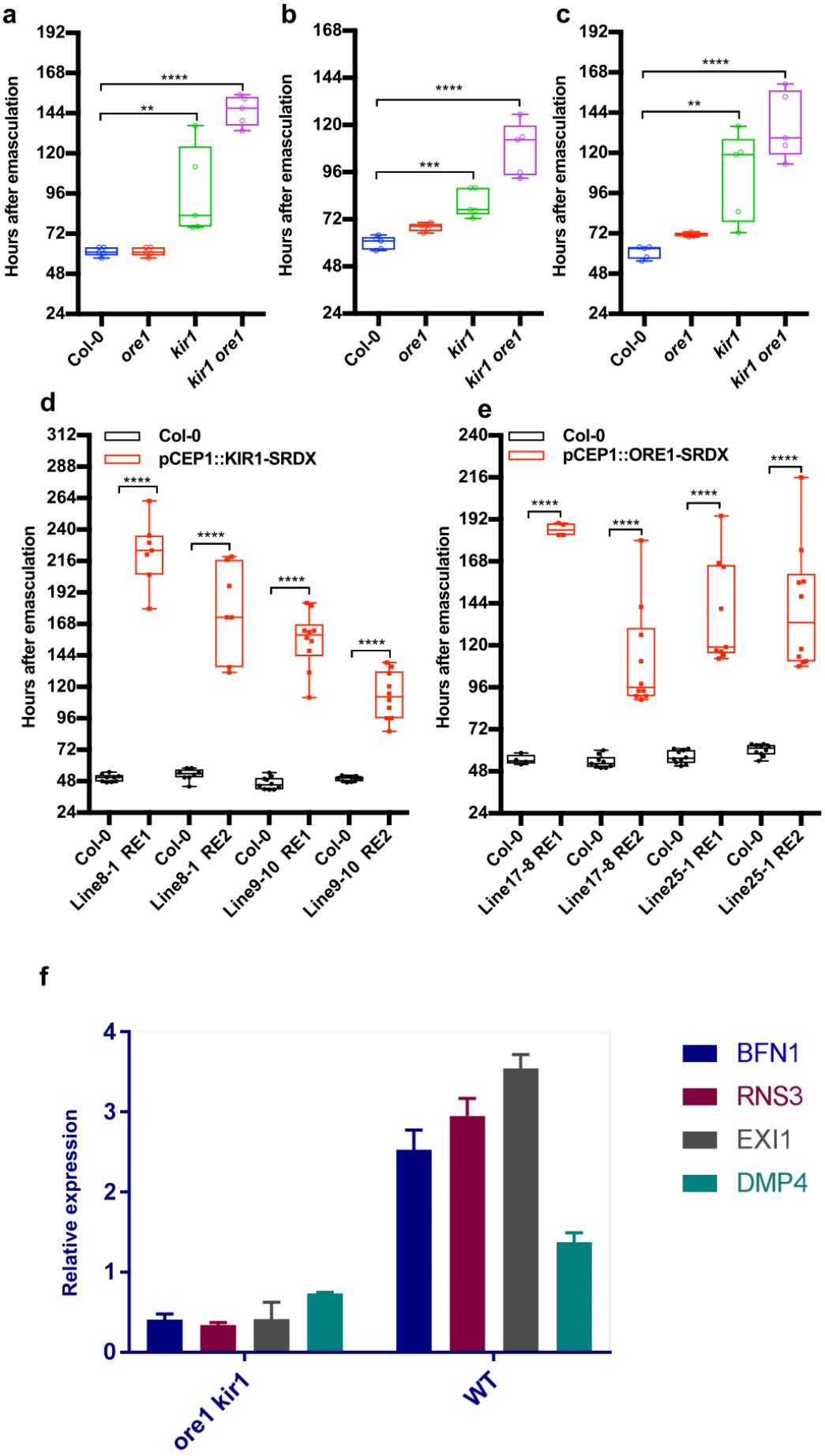
a
b
c
Hours after emasculation
Col-0
ore1
kir1
kir1 ore1
d
e
Col-0
pCEP1::KIR1-SRDX
pCEP1::ORE1-SRDX
Line8-1 RE1
Line8-1 RE2
Line9-10 RE1
Line9-10 RE2
Line17-8 RE1
Line17-8 RE2
Line25-1 RE1
Line25-1 RE2
f
Relative expression
BFN1
RNS3
EXI1
DMP4
ore1 kir1
WT

Figure S5. Individual webcam experiments to determine the onset of stigma collapse. a) – c) Three independent experiments visualizing the onset of stigma collapse in Col-0, *ore1*, *kir1* and *kir1 ore1* mutants. Whereas values vary from experiment to experiment, the significance tests provide a robust readout of genotype-dependent differences in stigma lifespan. n=5 for each box-and-whisker plot. **d)** Four independent experiments assessing the stigma longevity in two independent lines that harbor KIR1 fused to the EAR-like repressive domain SRDX (*KIR1-SRDX*). From left to right, Col-0 n = 9, 8, 10, 10; *KIR-SRDX* lines n = 7, 7, 10, 10. **e)** Four independent experiments assessing the stigma longevity in two independent *ORE1-SRDX* lines. From left to right, Col-0 n = 4, 9, 10, 10; *ORE1-SRDX* lines n = 4, 10, 9, 10. For every line, two biological repeats (RE1 and RE2) were performed. Statistical differences were calculated using two-way ANOVA with multiple comparisons by Fisher's LSD test, **p<0.01, *** p<0.001, ****p<0.0001. **f**) qPCR experiment shows upregulation of dPCD-associated genes in WT stigma versus stigma harvested from the double *ore1 kir1* mutant. The error bars represent SEM, n=2 biological replicates (200 stigmata per replicate); expression values are normalized to the reference genes ACTIN2 and EEF1A. All genes are significantly different at a significance level of p<0.005.

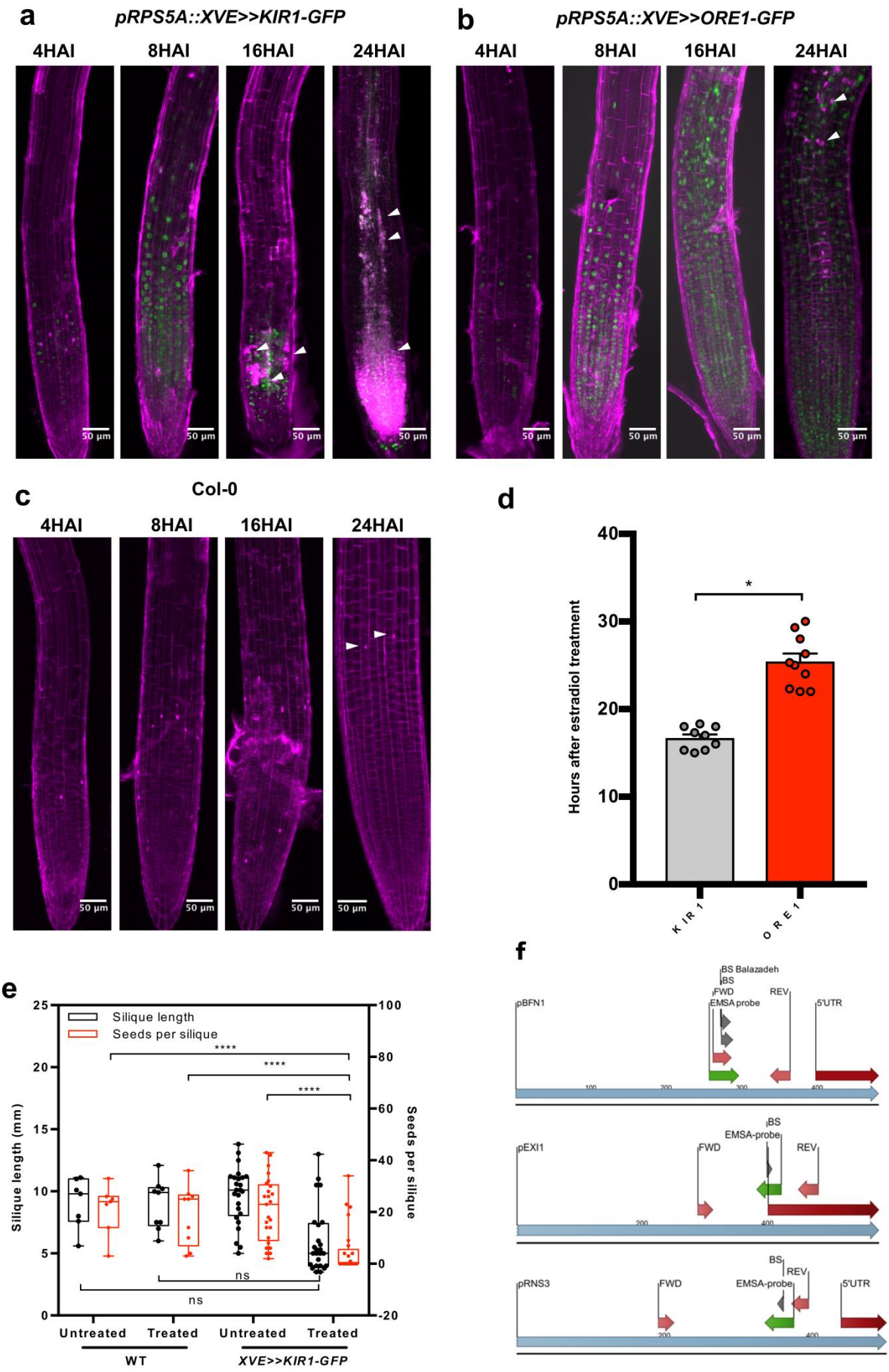
a
pRPS5A::XVE>>KIR1-GFP
4HAI
8HAI
16HAI
24HAI
50 µm
b
pRPS5A::XVE>>ORE1-GFP
4HAI
8HAI
16HAI
24HAI
50 µm
c
Col-0
4HAI
8HAI
16HAI
24HAI
50 µm
d
Hours after estradiol treatment
40
30
20
10
0
*
K I R 1
O R E 1
e
Silique length
Seeds per silique
Silique length (mm)
Seeds per silique
25
20
15
10
5
0
100
80
60
40
20
0
-20
****
****
****
ns
ns
Untreated
Treated
Untreated
Treated
WT
XVE>>KIR1-GFP
f
BS Balazadeh
BS
FWD
EMSA probe
REV
pBFN1
5'UTR
100
200
300
400
pEXI1
BS
EMSA-probe
FWD
REV
200
400
pRNS3
BS
REV
FWD
EMSA-probe
5'UTR
200
400

Figure S6: Induction of *KIR1-GFP* and *ORE1-GFP* induces cell death. a, b, c) Maximal projections of roots of 5-day-old estradiol-inducible *pRPS5A::XVE>>KIR1-GFP* (a), *pRPS5A::XVE>>ORE1-GFP* (b) and WT Col-0 (c) seedlings at 4-, 8-, 16-, and 24 h after estradiol induction (HAI). Note the presence of a nuclear GFP signal from 4 HAI onward in both lines. Arrowheads indicate PI-positive cells that undergo ectopic cell death from 16- (*KIR1-GFP*) or from 24 HAI onward (*ORE1-GFP*); in c), arrowheads mark the PI-positive nuclei of lateral root cap cells undergoing developmentally induced programmed cell death. Magenta - PI; green - GFP. Scale bars, 50 µm. **d)** Onset of root growth arrest in estradiol-treated 5-day-old seedlings from *pRPS5A::XVE>>KIR1-GFP* and *pRPS5A::XVE>>ORE1-GFP* lines (one representative line for each construct). Mean values are represented from left to right; n=9 (*KIR1*) and 10 (*ORE1*), respectively. Statistical differences were calculated using unpaired t-test, *=p<0.05. **e)** Seed set after estradiol treatment and pollination of *pCEP1::XVE>>KIR1-GFP* independent T1 lines. White box-and-whisker Tukey plots show the silique length (from left to right, mean±SD=9.029±2.032mm, 8.956±2.009mm, 9.668±2.285mm, 6.012±2.630mm, n=7,9,25,25.), grey box-and-whisker Tukey plots show the seeds per silique (from left to right, mean±SD=21.143±9.754, 18.889±11.516, 20.960±12.394, 5.040±9.280, N=7,9,25,25.). White circles and gray rectangles show outliers. Statistical differences were calculated using two-way ANOVA with multiple comparisons by Fisher's LSD test. ****=p<0.0001. **f)** Three diagrams indicating putative KIR1 binding sites in the promoters of the dPCD genes BFN1, EXI1 and RNS3. In the BFN1 promoter, "Balazadeh", indicates a binding site reported by *Matallana-Ramirez et al, 2013*. Binding sites selection and EMSA probe design are explained in detail in Materials & Methods.

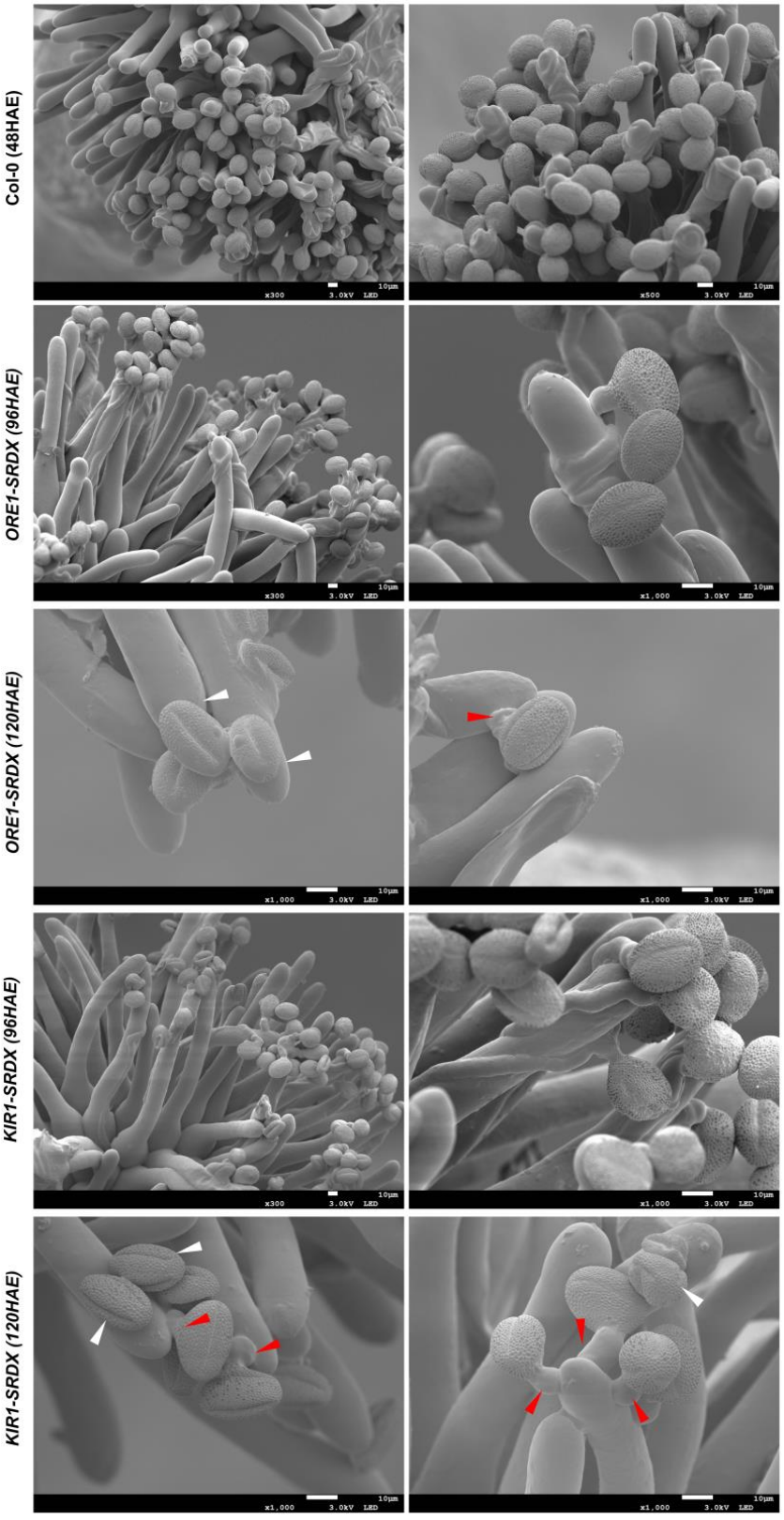

Figure S7: Pollen tube growth is impeded in late-senescent *ORE1-SRDX* and *KIR1-SRDX* stigmata.

Scanning electron micrographs of Col-0, *ORE1-SRDX* and *KIR1-SRDX* stigmata pollinated at 48 HAE (Col-0) and 96 and 120 HAE (SRDX-tagged lines). White arrowheads point at pollen grains, red arrowheads point at growing pollen tubes. Note the retarded pollen tube growth at 120 HAE in both *ORE1-SRDX* and *KIR1-SRDX* stigmata. Wild type Col-0 pollen from young flowers at anthesis was used for pollinations.

REFERENCES

1 Olvera-Carrillo, Y. *et al.* A conserved core of programmed cell death indicator genes discriminates developmentally and environmentally induced programmed cell death in plants. *Plant Physiol.* **169**, 2684-2699, doi:10.1104/pp.15.00769 (2015).

Supplementary table S2: Expression values of core dPCD genes and NAC transcription factor candidates upregulated during age-induced stigma senescence

Gene name	TAIR ID	Description	Stage 1a	Stage 2a	Stage 3a	LogFC21b	LogFC31c
CEP1	AT5G50260	Cysteine proteinases superfamily prot	5.75	233.62	2388.95	5.34	8.70
BFN1	AT1G11190	bifunctional nuclease 1	1.59	44.37	747.47	4.79	8.86
RNS3	AT1G26820	ribonuclease 3	4.3	126.84	2037.18	4.88	8.89
DMP4	AT4G18425	transmembrane protein, putative (DUF	3.37	201.2	2091.98	5.90	9.27
PASPA3	AT4G04460	Saposin-like aspartyl protease family	1.39	38.53	1232.91	4.79	9.79
EXI1	AT2G14095	hypothetical protein	0.47	11.87	268.67	4.64	9.14
SCPL48	AT3G45010	serine carboxypeptidase-like 48	11.52	225.14	3638.43	4.29	8.30
ANAC074	AT4G28530	NAC TF	0.47	25.32	284.58	5.69	9.18
ANAC041	AT2G33480	NAC TF	2.66	36.44	286.14	3.77	6.74
ANAC099	AT5G56620	NAC TF	0.33	7.71	35.93	4.52	6.74
ANAC047	AT3G04070	NAC TF	4.74	76.94	372.16	4.02	6.29
ANAC058	AT3G18400	NAC TF	0.09	1.32	6.46	3.77	6.05
ANAC083/VNI2	AT5G13180	NAC TF	1.87	13.38	119.7	2.83	5.99
ANAC059/ORS1	AT3G29035	NAC TF	0.9	18.15	52.48	4.32	5.85
ANAC092/ORE1	AT5G39610	NAC TF	7.34	57.82	349.63	2.98	5.57
ANAC010/SND3	AT1G28470	NAC TF	0.25	0.76	9.06	1.56	5.11
ANAC019	AT1G52890	NAC TF	21.85	145.13	617.37	2.73	4.82
ANAC087	AT5G18270	NAC TF	16.87	42.58	373.47	1.34	4.47
ANAC003	AT1G02220	NAC TF	2.08	8.74	45.65	2.07	4.45
ANAC021/022	AT1G56010	NAC TF	3.82	16.19	74.26	2.08	4.27
ANAC055	AT3G15500	NAC TF	9.56	40.95	153.71	2.10	4.01
ANAC029/AtNAP	AT1G69490	NAC TF	0.52	3.14	6.86	2.58	3.71
ANAC032	AT1G77450	NAC TF	0.55	0.57	5.61	0.07	3.33
ANAC056	AT3G15510	NAC TF	5.19	26.42	51.23	2.35	3.30

a: read counts averaged from 3 replicates
b: log2 fold change in expression level ; LogFC21 = Stage 2 vs. Stage 1
c: log2 fold change in expression level ; LogFC31= Stage 3 vs. Stage 1

Supplementary materials and methods:

Cloning and preparation of transgenic lines

The ToIM system and promoter-reporter lines for all dPCD-associated genes used in this article were published by Fendrych et al.[2] and Olvera-Carrillo et al[1], respectively. *KIR1* and *ORE1* coding sequences without stop codons were recombined into the pDONR221 vector (Invitrogen). The dominant-negative versions of *KIR1* and *ORE1* (*KIR1-SRDX* and *ORE1-SRDX)* were constructed by two-step PCR, and were recombined into the pDONR221 vector (Invitrogen). The 1.5-kb and 2.5-kb *proSLR1*, pro*UBQ10,* and pro*ORE1* promoter versions were isolated from Col-0 genomic DNA using specific primers and adding BamHI and XhoI restriction sites to clone directionally into pENTRL4-R1 (Invitrogen), a Gateway-compatible entry vector containing a cassette with multiple cloning sites (https://gateway.psb.ugent.be/). The *DT-A* coding sequence was derived from *pTH1* as described[3]. The *SLR1* promoter was assembled either with *DT-A* or *GFP* into the destination vector pB7m24GW,3 using LR Clonase II enzyme mix (Invitrogen). The *UBQ10* promoter[4] was assembled with ToIM into the destination vector pB7m24GW,3 using LR Clonase II enzyme mix (Invitrogen).

The 5-kb *KIR1* promoter was isolated from Col-0 genomic DNA and recombined into the pDONRP4P1r vector (Invitrogen). The 2.5-kb *ORE1* promoter was assembled by a multisite Gateway reaction using LR Clonase II+ enzyme mix (Invitrogen) with the *GAL4* coding sequence and the destination vector pB9-H2A-UAS-7m24GW to create activator lines as described[1]. These lines express a nuclear localized *GFP* reporter and can be used for *UAS-Gal4* transactivation as described[5]. The 1.5-kb *ORE1* and 5-kb *KIR1* promoters were assembled with pEN-L1-NF(NLSGFP)-L2, and pEN-R2-S(GUS)-L3 into the destination vector pB7m34GW as described[6]. The 1.5-kb ORE1 promoter was assembled with *ORE1* and *pEN-R2-F(GFP)-L3* into the destination vector pB7m34GW (Invitrogen). The 5-kb *KIR1* promoter was assembled with *KIR1-GFP-3'UTR* (synthesized by GenScript: http://www.genscript.com/) into the destination vector pB7m24GW,3. The promoter *CEP1* was

cloned upstream of *KIR1-SRDX* and *ORE1-SRDX* into the destination vector pB7m24GW,3. Primers used for PCR are listed in Supplementary Table 3.

The estradiol-inducible chimeric expression activator *XVE* was placed under the control of different promoters (*proRPS5A* and *proCEP1*) via PCR and classical cloning. The promoter fragments were amplified by PCR (Kpn1-CEP1-F and Xho1-CEP1-R for pCEP1; XhoI_RPS5A_FW and XhoI_RPS5A_REV for pRPS5A), followed by restriction digest, and ligated upstream of the *XVE* cassette in *pro1R4-ML-XVE*, and recombined into an expression vector as described[7] driving *ORE1-GFP* or *KIR1-GFP* fusion constructs. The cloned region and insertion orientation were sequence verified.

All expression clones obtained were transformed into *Agrobacterium tumefaciens* C58C1 (pMP90) or GV3101 (pMP90) competent cells using electroporation. Next these bacteria were used for a modified floral dip method to stably transform *Arabidopsis* plants, Col-0 ecotype. The bacteria were first grown for 6 h at 28 °C in 1 mL of non-selective YEB broth (pre-culture), then 10 mL of YEB was added and the culture was left at 28 °C overnight. Plants were dipped in the overnight culture after adding 40 mL of floral dip medium (10% sucrose, 0.05% Silwet L-77). T1 plants were selected on antibiotics or BASTA and segregation analysis was performed on T2 plants. All further analyses were performed with homozygous single-locus T3 plants, unless listed otherwise.

Camera systems

A high-quality SLR imaging system was set in a tissue growth chamber (24 h light, 20-22°C, humidity 50-65%), using a Canon EOS 650D camera controlled by Canon EOS Utility software, which was programmed to take an image every 30 min. For higher throughput, web-camera phenotyping systems were set up in a semi-controlled imaging environment (24 h light, 20-22°C, humidity 50-65%). Each system consisted of one computer and 10 Trust SpotLight Pro Web-cameras. Flowers were carefully positioned on handmade holders and set in front of the web-cameras. Each camera

records one picture every 10 min, allowing to follow 10 flowers in parallel. Two such systems were used for phenotyping experiments.

Sequence data processing and DEG analysis

After RNA-sequencing, the resulting BAM files were imported into the Galaxy Workflow Environment[8]. Sequencing data were sorted and the paired reads were mapped to genomic regions using an *A. thaliana* annotation file (TAIR10), a GFF3 format file downloaded from Ensembl Plants (http://plants.ensembl.org). To identify DEGs during stigma senescence, statistical analysis was carried out using edgeR package by R 3.3.1 in the graphical environment of RStudio (http://www.rstudio.com/)[9,10]. Read counts per gene locus were calculated from reads mapped to the genome. The expression genes were filtered as over 1 counts per million (CPM) present in at least three samples. The expression values were normalized by the "trimmed-mean of M-values" (TMM) normalization method. We defined DEGs as genes with a CPM value showing a ≥ 3-fold change in expression at a false discovery rate of ≤0.05 during stigma senescence. Gene annotations were added using Biomart Ensembl Plants (http://plants.ensembl.org/biomart/). Functional categorization of DEGs by gene ontology (GO) was performed using GO annotations from the TAIR website (http://www.*Arabidopsis*.org). GO term enrichment of DEGs was performed using DAVID (https://david.ncifcrf.gov/). Gene function classification was analyzed using MapMan 3.6. Cluster analysis of DEGs was performed using K-means clustering method in MeV 4.8.1 (http://mev.tm4.org/). The number of clusters was evaluated with the Figure-of-Merit algorithm implemented in MeV 4.8.1. Transcription factor identification and categorization was analyzed using AGRIS AtTFDB (http://*Arabidopsis*.med.ohio-state.edu/AtTFDB/). The complete RNA sequencing data set has been made publically available in ArrayExpress (https://www.ebi.ac.uk/arrayexpress; accession code E-MTAB-6279).

Tobacco infiltration

The *KIR1* and *ORE1* coding sequences were fused to the one of *GFP*, and placed under the control of the CaMV *35S* promoter in the destination vector pB7GW34. The truncated *KIR1* (1-252 AA) and *ORE1* (1-211 AA) were constructed in the destination vector pB7WG2D,1, which contains the endoplasmic reticulum *ER-GFP* marker as visible transfection control[11]. Tobacco (*Nicotiana tabacum*) plants were grown in soil for 4 to 6 weeks before infiltration with a suspension of transformed *A. tumefaciens* cells suspended at a cell density (OD600) of 1.5 in an infiltration medium (10 mM $MgSO_4$, 10 mM MES at pH 5.8, 100 µM acetosyringone).

qPCR

A total amount of 1 µg purified RNA was subjected to cDNA synthesis with the iScript cDNA synthesis kit (BioRad). The resulting cDNA was dissolved in ultra-pure water and mixed with the LightCycler 480 SYBR Green I Master (Roche) and 0.5 µM gene-specific primers (Supplementary Table 3) using JANUS automated pipetting station (Perkin Elmer). RT-qPCR was performed with a LightCycler system (Roche) in a program of 45 amplification cycles and primer annealing temperature of 60°C. RT-qPCR data was analyzed with Qbase+ software (BioGazelle, Belgium). Relative expression levels were calculated based on two reference genes (*ACTIN* and *EEF1A* for stigmata samples; *PEX4* and *UBL5* for seedlings).

Protein purification and EMSA

For protein expression and purification, the *ORE1* and *KIR1* coding sequences and *GFP* were recombined into the Gateway vector pDEST-HisMBP[12], and transformed into *Escherichia coli* strain BL21 (DE3). When cell density reached 0.6 (OD600), protein expression in 1-L cultures was induced at 18°C by addition of 1 mM isopropyl thio-β-D-galactoside in the course of 16 h. Cells were harvested by centrifugation. The cell pellet was resuspended in phosphate-buffered saline containing 5 mM DTT, 1% Triton X-100 and 0.75 $mg \cdot mL^{-1}$ lysozyme and incubated on ice for 30 min. Following sonication, the lysate was cleared by centrifugation at 10,000 g for 20 min. Ni-NTA agarose was used

for purification of His-tagged proteins by gravity-flow chromatography according to the protocol of the manufacturer. Concentrations of purified proteins were determined with the Pierce BCA Protein Assay Kit. EMSA probes using 5′-IRDye®700-labeled DNA fragments were synthetized by IDT (Supplementary Table 3). EMSAs were performed using the Odyssey infrared EMSA Kit from LI-COR following the manufacturer's protocol.

Cryo-SEM imaging

Optical and cryo-scanning electron microscopy (cryo-SEM) was utilized to study the microstructure of the samples. Optical microscopy was done on a Leica DM2500 microscope (Leica Micro-systems, Belgium). For cryo-SEM, samples of the emulsions were placed in the slots of a stub, plunge-frozen in slush nitrogen and transferred into the cryo-preparation chamber (PP3010T cryo-SEM Preparation System, Quorum Technologies, UK) where they were freeze-fractured, sublimated for 20 min and subsequently sputter-coated with platinum and examined by a JEOL JSM 7100F SEM (JEOL Ltd, Tokyo, Japan).

Statistical analysis, image analysis and figure preparation

Statistical data were analyzed in Graphpad Prism 7 (GraphPad Software, La Jolla California USA, www.graphpad.com). Statistical images were generated by Graphpad Prism 7. Camera and confocal images were prepared with ImageJ (http://imagej.nih.gov/ij/)[13], the only manipulation of images were histogram adjustments. The figures were then assembled in Inkscape (https://inkscape.org).

References:

1 Olvera-Carrillo, Y. *et al.* A Conserved Core of Programmed Cell Death Indicator Genes Discriminates Developmentally and Environmentally Induced Programmed Cell Death in Plants. *Plant physiology* **169**, 2684-2699, doi:10.1104/pp.15.00769 (2015).

2 Fendrych, M. *et al.* Programmed cell death controlled by ANAC033/SOMBRERO determines root cap organ size in *Arabidopsis*. *Current Biology* **24**, 931-940, doi:10.1016/j.cub.2014.03.025 (2014).

3 Weijers, D., van Hamburg, J.-P., van Rijn, E., Hooykaas, P. J. J. & Offringa, R. Diphtheria toxin-mediated cell ablation reveals interregional communication during Arabidopsis seed development. *Plant Physiol.* **133**, 1882-1892, doi:10.1104/pp.103.030692 (2003).

4 Grefen, C. *et al.* A ubiquitin-10 promoter-based vector set for fluorescent protein tagging facilitates temporal stability and native protein distribution in transient and stable expression studies. *Plant J.* **64**, 355-365, doi:10.1111/j.1365-313X.2010.04322.x (2010).

5 Karimi, M., De Meyer, B. & Hilson, P. Modular cloning in plant cells. *Trends in plant science* **10**, 103-105, doi:10.1016/j.tplants.2005.01.008 (2005).

6 Karimi, M., Bleys, A., Vanderhaeghen, R. & Hilson, P. Building blocks for plant gene assembly. *Plant physiology* **145**, 1183-1191, doi:10.1104/pp.107.110411 (2007).

7 Siligato, R. *et al.* MultiSite Gateway-Compatible Cell Type-Specific Gene-Inducible System for Plants. *Plant physiology* **170**, 627-641, doi:10.1104/pp.15.01246 (2016).

8 Afgan, E. *et al.* The Galaxy platform for accessible, reproducible and collaborative biomedical analyses: 2016 update. *Nucleic Acids Res.* **44**, W3-W10, doi:10.1093/nar/gkw343 (2016).

9 Ihaka, R. & Gentleman, R. R: A language for data analysis and graphics. *J. Comput. Graph. Stat.* **5**, 299-314, doi:10.1080/10618600.1996.10474713 (1996).

10 Zhou, X., Lindsay, H. & Robinson, M. D. Robustly detecting differential expression in RNA sequencing data using observation weights. *Nucleic Acids Res.* **42**, e91, doi:10.1093/nar/gku310 (2014).

11 Karimi, M., Inzé, D. & Depicker, A. GATEWAY^{TM} vectors for *Agrobacterium*-mediated plant transformation. *Trends in plant science* **7**, 193-195, doi:10.1016/S1360-1385(02)02251-3 (2002).

12 Nallamsetty, S., Austin, B. P., Penrose, K. J. & Waugh, D. S. Gateway vectors for the production of combinatorially-tagged His_6-MBP fusion proteins in the cytoplasm and periplasm of *Escherichia coli*. *Protein Science* **14**, 2964-2971, doi:10.1110/ps.051718605 (2005).

13 Schneider, C. A., Rasband, W. S. & Eliceiri, K. W. NIH Image to ImageJ: 25 years of image analysis. *Nature Methods* **9**, 671-675, doi:10.1038/Nmeth.2089 (2012).